IOP Publishing Superconductor Science and Technology
Supercond. Sci. Technol. 31 (2018) 045003 (7pp) https://doi.org/10.1088/1361-6668/aaab20

Negative inductance SQUID qubit operating in a quantum regime

W Y Liu[1,2,3], F F Su[1,3], H K Xu[1,3], Z Y Li[1,4], Ye Tian[1], X B Zhu[1,6], Li Lu[1], Siyuan Han[1,2,7] and S P Zhao[1,3,5,7]

[1] Beijing National Laboratory for Condensed Matter Physics, Institute of Physics, Chinese Academy of Sciences, Beijing 100190, People's Republic of China
[2] Department of Physics and Astronomy, University of Kansas, Lawrence, KS 66045, United States of America
[3] School of Physical Sciences, University of Chinese Academy of Sciences, Beijing 100049, People's Republic of China
[4] National Laboratory of Solid State Microstructures, School of Physics, Nanjing University, Nanjing 210093, People's Republic of China
[5] Collaborative Innovation Center of Quantum Matter, Beijing, People's Republic of China

E-mail: han@ku.edu and spzhao@iphy.ac.cn

Received 20 November 2017, revised 23 January 2018
Accepted for publication 29 January 2018
Published 21 February 2018

Abstract

Two-junction SQUIDs with negative mutual inductance between their two arms, called nSQUIDs, have been proposed for significantly improving quantum information transfer but their quantum nature has not been experimentally demonstrated. We have designed, fabricated, and characterized superconducting nSQUID qubits. Our results provide clear evidence of the quantum coherence of the device, whose properties are well described by theoretical calculations using parameters determined from spectroscopic measurement. In addition to their future application for fast quantum information transfer, the nSQUID qubits exhibit rich characteristics in their tunable two-dimensional (2D) potentials, energy levels, wave function symmetries, and dipole matrix elements, which are essential to the study of a wide variety of macroscopic quantum phenomena such as tunneling in 2D potential landscapes.

Keywords: superconducting qubit, negative inductance SQUID, quantum information transfer, artificial atom

(Some figures may appear in colour only in the online journal)

Introduction

Superconducting qubits have emerged as one of the leading candidates for building solid-state quantum computers (SQC) [1, 2]. In addition to qubit coherence times, of which significant progress has been achieved recently, scalable fault-tolerant circuit-model quantum computation requires a rapid transfer of quantum information among a large number of qubits. A novel method of quantum information transmission (QIT) in superconducting quantum circuits based on the quantum dynamics of magnetic flux in SQUIDs has been proposed to address this important issue [3]. The main element of this novel approach is the use of dual-rail arrays of negative-inductance SQUIDs (nSQUIDs), which have the potential to result in a significant improvement over the current state-of-the-art in QIT. At the present time, QIT between qubits is realized either by controllable coupling between qubits or qubit–qubit interaction mediated by qubit-microwave cavity interaction. This type of QIT has several drawbacks which may reduce its usefulness in SQC. The first one is the relatively slow speed of QIT which is fundamental in nature. For example, two swap operations are needed to transfer an arbitrary quantum state from one qubit to another via a microwave cavity, which requires about tens of ns to complete because the time scale required to transfer quantum

[6] Present address: CAS Center for Excellence and Synergetic Innovation Center in Quantum Information and Quantum Physics, University of Science and Technology of China, Hefei, Anhui 230026, People's Republic of China.
[7] Author to whom any correspondence should be addressed.

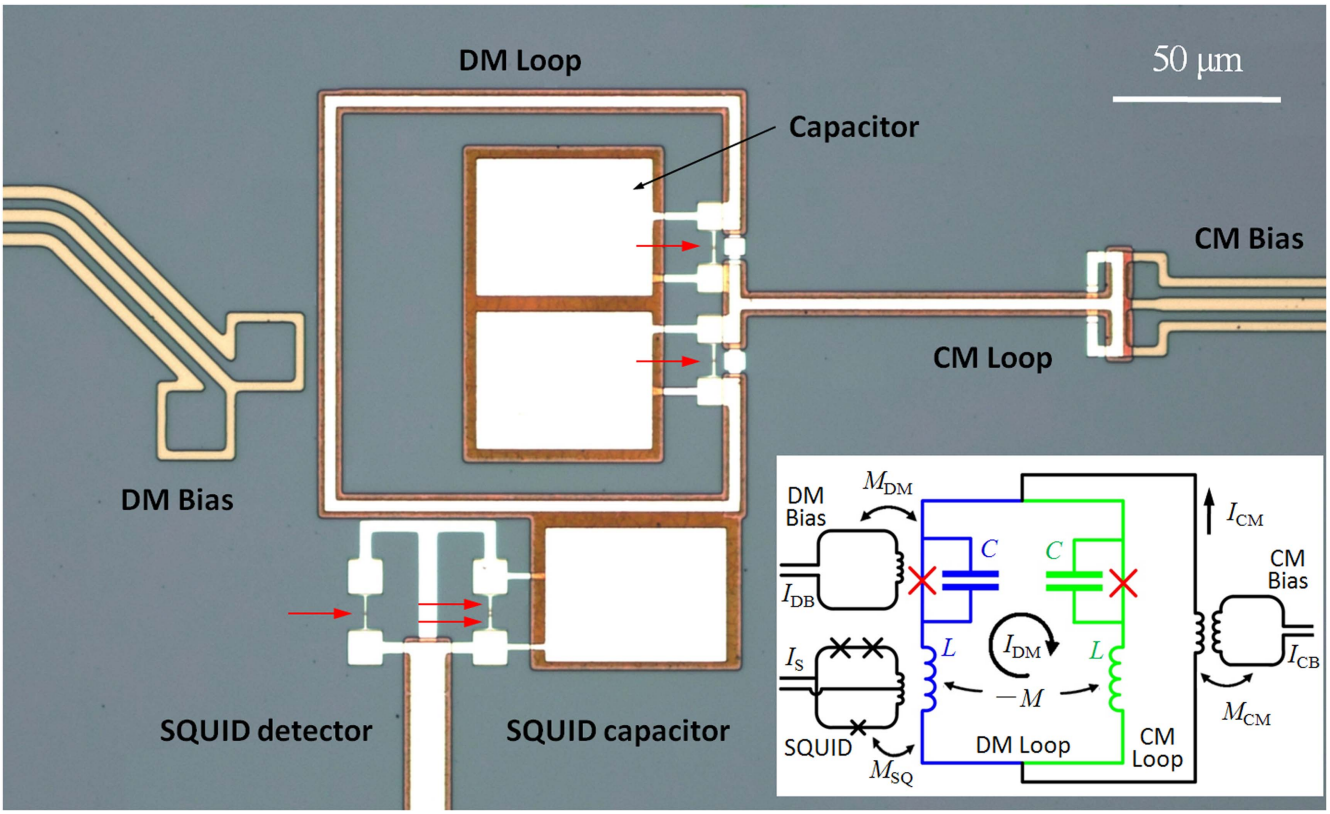

Figure 1. False-colored optical photograph of the central part of the qubit with the substrate, Nb layer, Al layers, and α-Si layer appearing in gray, light yellow, white, and brown, respectively. Similar Al film structures exist beneath the α-Si insulating layer, not seen in the figure, as those on top of it. Each red arrow points to the place where a shadow evaporated Al junction locates. Inset shows the nSQUID qubit schematic with Josephson junctions (red crosses), capacitances C, and inductances L for each qubit arms (green and blue). The mutual inductance between the two arms is $-M < 0$. The bias and circulating currents of CM (common mode) and DM (differential mode) and various mutual inductances are indicated.

Table 1. Sample parameters with current, capacitance, and inductance in μA, fF, and pH, respectively. M_{CM} (M_{DM}) is the mutual inductance between the qubit and common (differential) mode bias loop. Fitted parameters are obtained with unchanged l.

	I_c	C	L	M	l	β	M_{DM}	M_{CM}
Designed	2.66	1100	468	372	45	6.8	2.34	1.11
Fitted	2.61	1325	472	383	45	6.79	2.15	1.18

information between qubits and cavities is inversely proportional to the strength of qubit-cavity interaction which is significantly weaker than that between qubits and microwave fields. Though this is acceptable for QIT between the nearest neighbors, it could be too slow for QIT in more complex circuits, where it would require many cascaded operations. The second drawback is that in circuits with more than two qubits, QIT via a microwave cavity needs either a rapid switching on and off of the qubit-cavity coupling, or strong separation of the qubit frequencies. Both of these obstacles make it difficult to scale up such circuits to more than a few tens of qubits. In contrast, the dual-rail QIT protocol based on arrays of nSQUIDs provides the basis for a scalable QIT architecture, and thus can solve the main problems of microwave-cavity-mediated quantum state transfer mentioned above.

The circuits of nSQUIDs have two degrees of freedom, namely the differential mode (DM) and the common mode (CM), which can be used to encode and transport quantum information, respectively [3–8]. They can be operated either as phase qubits or flux qubits. When operated as phase qubits their double-well potential is significantly tilted and the two lowest energy levels in the same potential well are used as the computational basis states. In contrast, nSQUIDs operated as flux qubits have near symmetric double-well potential with suitable barrier height so that the bottom levels in the potential wells are used as basis states. Although the design and operation of nSQUIDs have been validated in classical superconducting reversible computing, the quantum nature of these devices, in particular coherence, still must be demonstrated experimentally first for applications of nSQUID-based architectures in quantum information processing [8, 9].

In this paper, we present the design, fabrication, and characterization of the nSQUID qubits operating in the quantum regime. The device quantum coherence is clearly

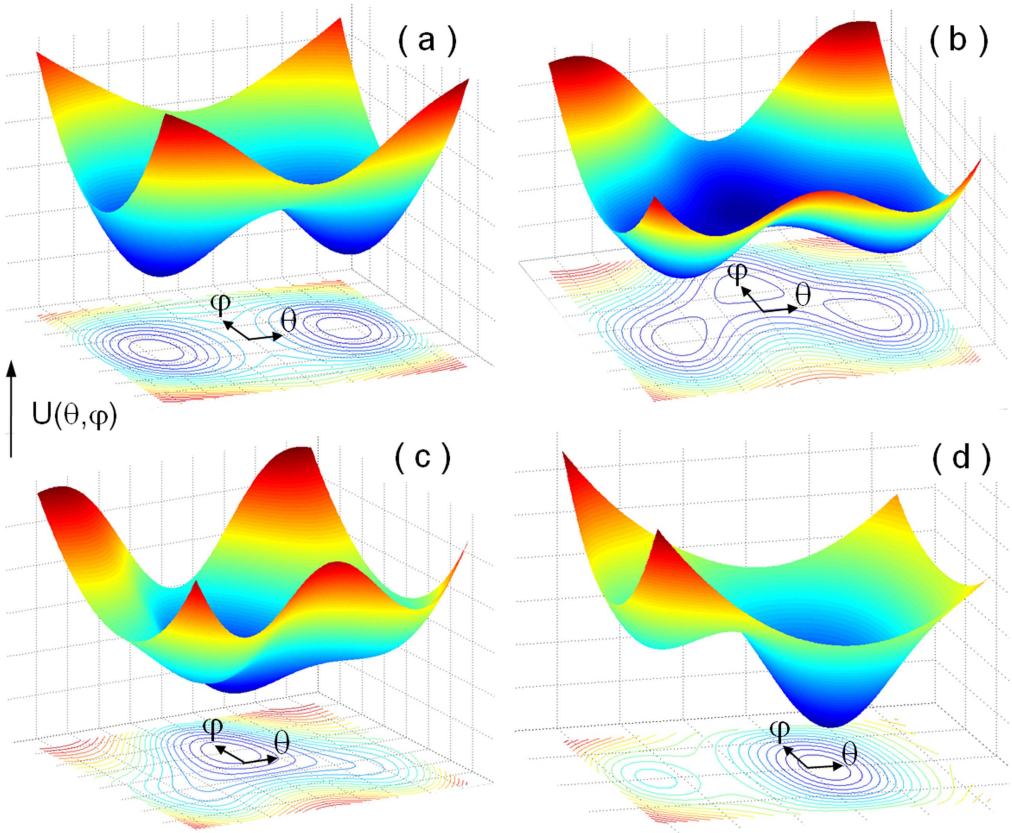

Figure 2. Typical 2D potential landscapes of the nSQUID qubit. (a) Symmetric double well with $\varphi_e/2\pi = 0$ and $\theta_e/2\pi = 0.5$, (b) three wells with $\varphi_e/2\pi = 0.37$ and $\theta_e/2\pi = 0.5$, (c) single well at $\varphi_e/2\pi = 0.6$ and $\theta_e/2\pi = 0.5$, and (d) asymmetric double well at $\varphi_e/2\pi = 0$ and $\theta_e/2\pi = 0.9$.

demonstrated experimentally, with the nSQUID qubits operating in the phase mode. Our results provide the basis for the further studies and development of nSQUID qubits for fast quantum information transfer applications.

The qubit Hamiltonian

As schematically depicted in the inset of figure 1, the nSQUID qubit can be seen as a two-junction SQUID with negative mutual inductance $-M < 0$ between its two arms each having self inductance L as drawn in green and blue [3–6, 8]. The junctions indicated by the two crosses are identical each with Josephson critical current I_c and shunt capacitance C. The qubit has two degrees of freedom: the CM represents the total current I_{CM} flowing through the two junctions of the SQUID and the DM represents circulation current I_{DM} indicated in the inset of figure 1. This system of two degrees of freedom can be viewed as a 'fictitious flux particle' with effective masses C_D and C_C, momenta Q_D and Q_C, and coordinates θ and ϕ moving in a two-dimensional (2D) potential energy landscape $U(\theta, \phi)$ [10]. The Hamiltonian of the nSQUID can be written as [8]

$$H = \frac{Q_C^2}{2C_C} + \frac{Q_D^2}{2C_D} + U(\theta, \varphi) \tag{1}$$

with $C_C = C/2$, $C_D = 2C$, and $Q_C = (Q_1 + Q_2)/2$, $Q_D = Q_1 - Q_2$, where $Q_{1,2}$ are the charges on the shunt capacitors of the two junctions. Also we have defined the DM variable $\theta = (\phi_1 - \phi_2)/2$ and the CM variable $\varphi = \phi_1 + \phi_2$ with $\phi_{1,2}$ being phase differences across the two junctions. The potential in equation (1) is given by

$$U(\theta, \varphi) = \frac{{\Phi_0}^2}{2\pi^2(L+M)}\left[\frac{1}{2}(\theta - \theta_e)^2 - \beta\cos\frac{\varphi}{2}\cos\theta + \frac{1}{8}\frac{L+M}{L-M}(\varphi - \varphi_e)^2\right], \tag{2}$$

where Φ_0 is the magnetic flux quantum, $\beta = 2(L+M)I_c/\Phi_0$, $\theta_e/2\pi$ and $\varphi_e/2\pi$ are DM and CM flux biases in units of Φ_0, respectively. The effective inductances for the common and differential modes are $L_C = (L-M)/2$ and $L_D = 2(L+M)$, respectively.

Qubit fabrication

For fast quantum information transfer L_C should be made as small as possible, namely with M approaching L. In order to maximize M, the two arms of the qubit loops were designed to have the same dimension and lay on top of each other with a Si insulating layer separating them. Figure 1 shows the false-

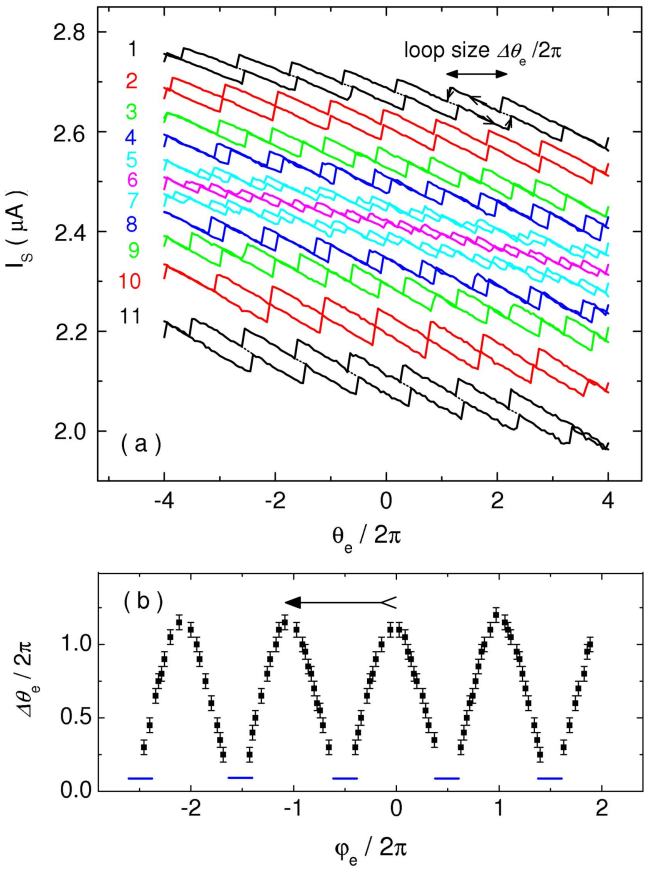

Figure 3. Switching current I_S of the SQUID detector versus DM bias θ_e for several CM bias φ_e, showing the hysteresis loops that reflect different qubit potential well structure and barrier height. The curves from 1 to 11 are obtained with the flux bias $\varphi_e/2\pi$ of 0.058, −0.093, −0.244, −0.334, −0.425, −0.485, −0.545, −0.636, −0.726, −0.877, and −1.058, respectively. Short dotted lines in curves 1 and 11 are guides for the eye. Arrows in trace 1 show an example of the scan directions. (b) The horizontal size of the loops shown in (a) as a function of CM bias plotted in a wider range, demonstrating a tunable periodic variation of the potential barrier height. Small horizontal bars near the bottom indicate the φ_e range in which three well structures appear. The leftward arrow indicates the $\varphi_e/2\pi$ range for the curves 1–11 in (a).

colored optical photograph of the core area of the fabricated device. For the sample fabrication, we used Si wafers of 2 inches in diameter and 0.38 mm in thickness with sixteen 6×6 mm^2 chips having identical devices designed near the center and cut apart after the fabrication process was completed. Si wafers with oxidized surface were used in this first study, which made the later dry etching of the Nb and α-Si films in SF_6 much convenient due to the extremely low etching rate of the surface oxidized Si layer.

The outer circuits of the nSQUID qubit were fabricated first by dc sputtering a 150 nm Nb film (colored as light yellow in the figure) followed by photolithographical patterning and reactive ion etching in SF_6. Subsequent processes included two layers of Al films prepared by e-beam lithographical patterning, evaporation, and lift-off. The intermediate α-Si layer was grown by plasma enhanced chemical vapor deposition (PECVD) in SiH_4 and Ar gas mixture at elevated temperature [11], patterned by e-beam lithography, and etched in SF_6. Finally, the Josephson junctions in both the qubit and the three-junction dc-SQUID qubit-state detector, as pointed by the horizontal arrows in figure 1, were formed by double-angle shadow evaporation. Shunt capacitors were used to reduce the qubit level spacing to the range of microwaves and increase flux resolution of the SQUID detector. Detailed fabrication processes similar to those for the present device are described in [11].

For the device shown in figure 1, the ratio of $M/L \rightarrow M/(L + l)$ is calculated to be 0.73 taking into account the contribution to L from the inductance l indicate in figure 1 of the two small loops in the qubit used for CM flux bias on the right side of the figure. M/L can be made as high as 0.81 if the CM is current biased ($l \sim 0$) as shown in the inset. In table 1, the designed device parameters are listed together with those which are used to obtain good fits to the experimental results (see below).

Figure 2 shows the four typical structures of the qubit potential defined by equation (2) and plotted using the best-fit parameters listed in table 1. In figure 2(a), we have $\varphi_e = 0$ and $\theta_e = \pi$. From the figure and also from equation (2), we see that if $\varphi_e = 0$, a cut by the plane $\varphi = 0$ would lead to a 1D potential $U(\theta, 0) \sim (\theta - \theta_e)^2/2 - \beta\cos\theta$, corresponding to that of the well-known rf-SQUID phase qubit [12]. A nonzero φ then leads to a 2D potential with additional parabolic dependence in the φ direction, resulting in a saddle point at $\theta = \varphi = 0$, which is the lowest point of the barrier separating the two potential wells, as can be seen in figure 2(a). There are two consequences as φ_e is increased gradually from zero. First, the saddle point will move toward the point of $\theta = 0$ and $\varphi \approx \varphi_e$. Second, since θ is the degree of freedom that encodes quantum information, the prefactor $\beta\cos\varphi/2$ before $\cos\theta$ in equation (2) acts as an effective $\beta_{\rm eff}$ which is $\sim\beta\cos\varphi_e/2$, so that the potential barrier of the nSQUID can be tuned *in situ* by varying φ_e. Furthermore, decreasing $\beta_{\rm eff}$ makes the potential wells more asymmetric with respect to the plane of φ mod $4\pi = 0$, which results in curved tunneling path connecting the two potential wells. As φ_e is increased further, a third potential well emerges, as depicted in figure 2(b). Finally the original two wells merge into the middle well leaving a single-well potential as shown in figure 2(c). On the other hand, keeping $\varphi_e = 0$ and increasing θ_e tilts the potential as shown in figure 2(d). In this case, the potential is symmetric (symmetric) with respect to the $\varphi = 0$ ($\theta = 0$) plane.

Results and discussion

The properties discussed above were experimentally verified in the present nSQUID qubit. Our measurements were performed in an Oxford cryogen-free dilution refrigerator at 10 mK with circuitry featuring various filtering, shielding, and attenuation, which is suitable for detecting the qubit coherence properties [13, 14]. The dc-SQUID detector was used to readout the nSQUID qubit state. The switching current I_s of the SQUID is sensitive to the total magnetic flux

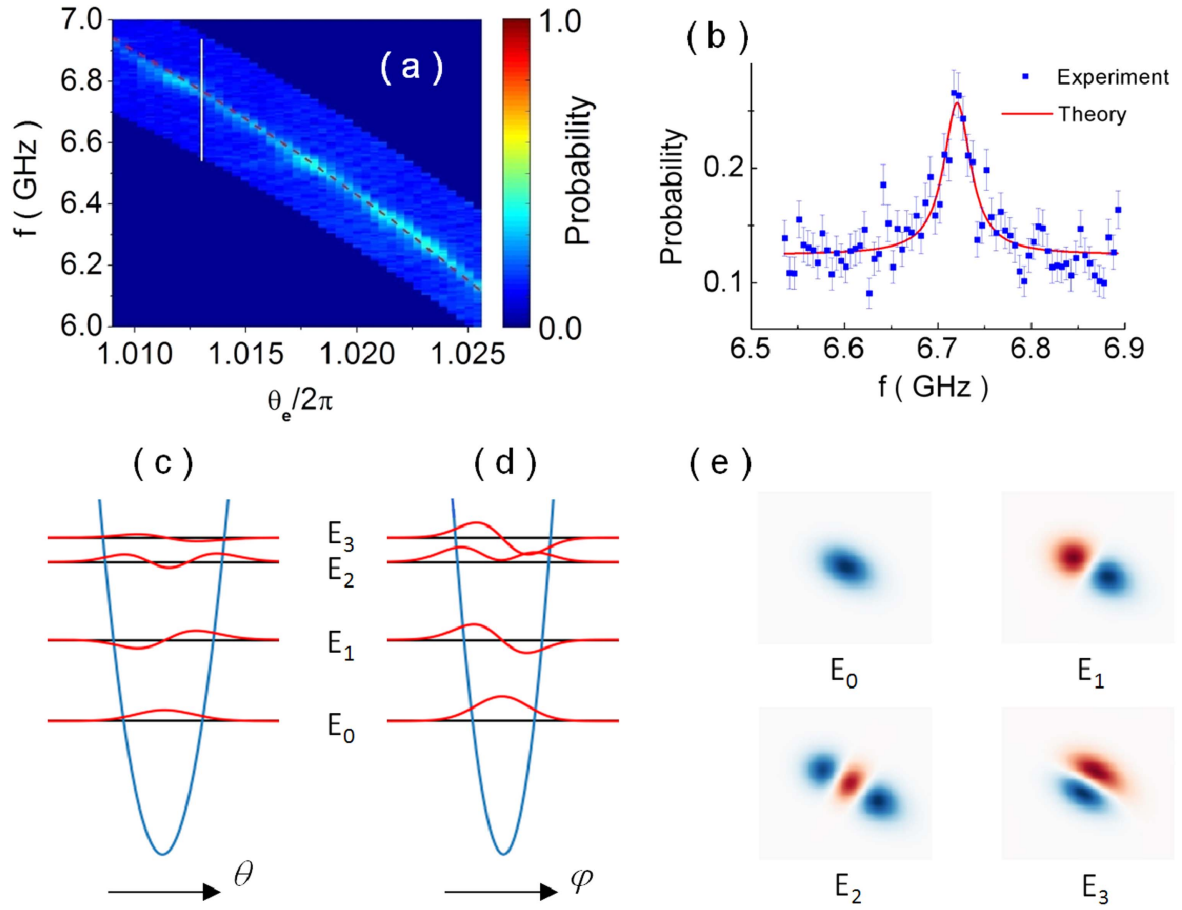

Figure 4. (a) Experimental energy spectrum measured at $\varphi_e/2\pi = 0.210$. The dashed line shows the calculated result. (b) The nSQUID qubit excited probability versus microwave frequency measured at $\varphi_e/2\pi = 0.210$ and $\theta_e/2\pi = 1.013$ along the white line in (a) with statistical error bar of 2σ. (c) The bottom four energy levels (black) and wave functions (red) along the θ axis after integrating over φ and (d) those along the φ axis after integrating over θ, calculated with the same flux biases and using the fitted parameters listed in table 1. (e) Calculated wave functions corresponding to the four energy levels, plotted in two dimensions (horizontal: θ, vertical:φ) with plus (blue) and minus (red) signs.

Φ_{SQ} threading the SQUID loop:

$$\Phi_{SQ} = M_{SQ} I_{DM} + M' I_{CB} + M'' I_{DB} , \quad (3)$$

where M_{SQ} is the mutual inductance between the SQUID and the qubit's DM loop, as indicated in the inset of figure 1. I_{CB} and I_{DB} are the CM and DM flux bias currents, respectively. $M'(M'')$ is the mutual inductance between the CM (DM) flux bias line and the SQUID loop, which can be estimated from the readout SQUID's flux-I_s transfer function. Notice that by geometry of the design I_{CM} is decoupled from the SQUID. In equation (3), I_{DM} is the circulating DM current which depends on the fluxoid state of the differential mode, thus the fluxoid state of differential mode can be inferred from switching current of the SQUID. In figure 3(a), we show the switching current I_S as a function of the DM bias θ_e for several CM bias φ_e ranging from 0 to -2π as indicated by a leftward arrow in figure 3(b). The hysteresis loops in I_S versus θ_e can be clearly seen in figure 3(a). For curve 1, for instance, we set $\varphi_e = 0$ and when θ_e was swept from left to right (upper part) and back (lower part) there is clear hysteresis. Each jump in the curve signals the fictitious flux particle tunneling from one potential well to the next as the potential is tilted by changing θ_e (see figure 2(d)). The size of the hysteresis loop $\Delta\theta_e/2\pi$, as indicated in figure 3(a), scales roughly with the potential barrier height. The θ versus θ_e relation is therefore multi-valued with the hysteresis loops $\Delta\theta_e/2\pi$ increasing with increasing β [15]. In figure 3(a), we can see that the hysteresis loops size $\Delta\theta_e/2\pi$ decreases as $|\varphi_e|$ is increased from 0 (curves 1–4), due to decreasing β_{eff}. The overall negative slope of θ versus θ_e for fixed values of φ_e is due to the cross talk from I_{DB} (the second term on the left side of the equation (3)). The vertical shift between individual I_S versus θ_e curves are due to the cross talk from I_{CB} of the third term on the left hand side of equation (3).

As φ_e is increased further, each single hysteresis loop starts to split into two smaller loops (curve 5 in figure 3) which further move apart gradually (curve 6 in figure 3). Due to the emergence of the third potential well between the original two wells as shown in figure 2(b), we can see from figure 3(a) that increasing φ_e further (curves 7–11) results in the change of the hysteresis loop size $\Delta\theta_e/2\pi$ in a periodic manner as expected. The periodic structures of individual θ_e scans in figure 3(a) were used to calibrate the relationship of DM bias current I_{DB} and external flux θ_e. In figure 3(b), we

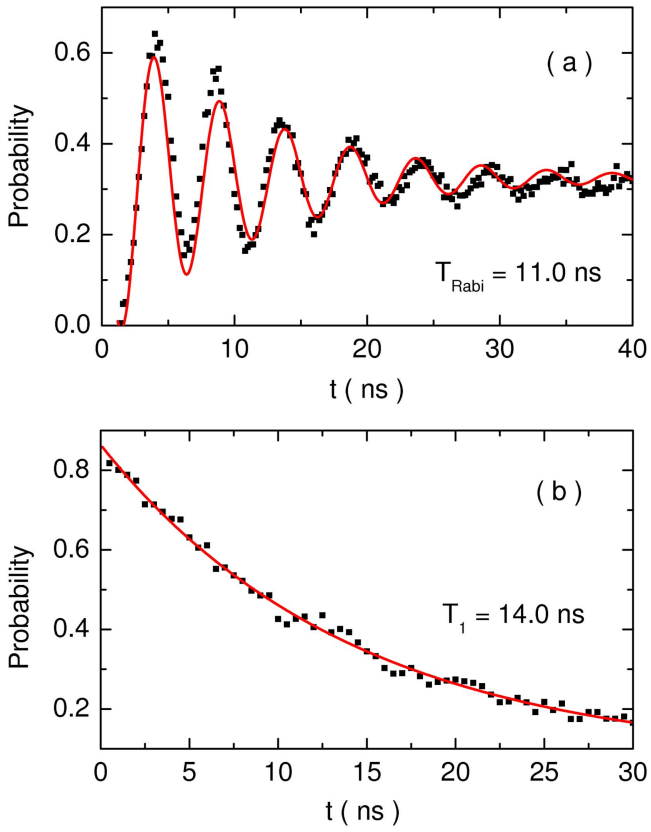

Figure 5. (a) Rabi oscillation measured at $\varphi_e/2\pi = 0.210$ and $\theta_e/2\pi = 1.013$ for the nSQUID qubit. (b) The energy relaxation of the nSQUID qubit measured at the same bias point.

show the φ_e-dependence of the size of the hysteresis loops in a wider range, in which a periodic dependence can be clearly seen which was also used to calibrate the CM external flux bias φ_e.

The energy spectrum of the nSQUID qubit was measured by changing θ_e to tilt the two potential wells while keeping φ_e constant as shown in figure 2(d). The measurement was carried out by sending a 4 μs microwave pulse, and measuring the excited-state population right after the microwave was turned off. The flux bias and microwave frequency were swept with steps of $0.4\,\mathrm{m}\Phi_0$ and 5 MHz, respectively. Figure 4(a) shows the result obtained at $\varphi_e/2\pi = 0.210$ and $1.009 < \theta_e/2\pi < 1.0256$. Figure 4(b) shows that the nSQUID qubit was excited with the microwave. The resonant peak was fitted to a Lorentzian function, yielding center frequency of 6.71 GHz and FWHM = 36 MHz at $\varphi_e/2\pi = 0.210$ and $\theta_e/2\pi = 1.013$. The experimental spectrum fits very well with the numerical calculations (the red dash line as shown in figure 4(a)) by using equations (1) and (2) and adjusting the nSQUID parameters around their designed values. The calculations were performed using the Fourier grid Hamiltonian method [16], from which the energy levels and wave functions of the 2D system were obtained. Also from the maximum loop size discussed above we obtain a $\beta = 6.79$. The experimentally fitted sample parameters are listed in table 1. The numerical calculated qubit transition frequency $f_{10} = (E_1 - E_0)/h$ is very sensitivity to nSQUID parameters, where E_i is the ith energy level of the qubit. For example, changing the value of β from 6.79 to 6.80 results in about +55 MHz frequency shift.

Quantum coherence was clearly demonstrated by observing Rabi oscillation as shown in figure 5(a) at $\varphi_e/2\pi = 0.210$ and $\theta_e/2\pi = 1.013$. At this biases, a short resonant microwave pulse of variable length with frequency $f_{10} = 6.711$ GHz was applied, which coherently transferred population between the ground state and the first excited state. By fitting the experimental data, we find the coherence time $T_{\mathrm{Rabi}} = 11$ ns. The relaxation time was obtained from the usual pump-probe measurement to be $T_1 = 14$ ns as shown in figure 5(b). The coherence time is quite short which partly results from the lossy ($\tan\delta > 10^{-4}$) PECVD deposited α-Si layer used to separate the two vertically stacked arms of the nSQUID DM loop (with an overlapping area of 2880 $\mu\mathrm{m}^2$). Two-level defects in this α-Si layer couple strongly to the DM dynamics of the nSQUID causing severe decoherence [11]. In addition, the Si substrate with oxidized surface should also contribute significantly to the decoherence [17–21]. To improve the qubit coherence, it is necessary to optimize the growth condition of PECVD α-Si to reduce loss tangent and the density of two-level defects. Sapphire or unoxidized Si substrates with careful surface treatment [17–21] will be used in future studies.

Figures 4(c) and (d) show the bottom four energy levels (black) as well as the wave functions (red) along the θ- and φ-axis after integrating over the other axis, respectively. The results are calculated at the same flux biases of $\varphi_e/2\pi = 0.210$ and $\theta_e/2\pi = 1.013$ used for the Rabi measurement in figure 5(a). For the bottom three levels, the relative anharmonicity α of the system is about 4%. We find that α can be adjusted from 3% to greater than 30% by changing θ_e and therefore the depth of the potential well. In figure 4(d), we show the wave functions at the same flux biases plotted in two dimensions (horizontal: θ, vertical: φ) with plus (blue) and minus (red) signs. An interesting feature is that in general the axes of symmetry of the wave functions are not parallel to the θ- or φ-axis. As can be seen in figure 2(a), when $\varphi_e = 0$ and $\theta_e = 0.5$, the qubit potential is symmetric with respect to the θ- and φ-axis, and the wave functions have well defined parities. When $\varphi_e/2\pi \neq 0$ and $\theta_e/2\pi \neq 0.5$, on the other hand, the symmetry along the ϕ and θ directions of the qubit potential is broken (e.g. figure 2(b)) and the wave functions become asymmetric (e.g. figure 4(e)). Hence, the dipole matrix elements (or transition rates) between various eigenstates depend critically on the values of φ_e and θ_e. The rich structures of the energy levels and wave functions, including the tunable anharmonicity and tunable transition rates between any two qubit states [22], are advantageous in the studies of macroscopic quantum phenomena using superconducting artificial atoms. In addition, the rich structure of the potential can be used to investigate macroscopic quantum tunneling in a 2D potential energy landscapes [23–25].

Summary

We have designed, fabricated, and characterized the superconducting nSQUID qubits. Most importantly, we have experimentally demonstrated the quantum coherence of nSQUID qubits. Our results provide the basis for the future studies of the device in fast quantum information transfer with further improvement of the coherence property. In addition, the nSQUID qubits exhibit rich characters in their tunable two-dimensional potentials, energy levels, and wave function symmetries and dipole matrix elements, which can be useful in various applications as artificial atoms.

Acknowledgments

We thank the Laboratory of Microfabrication at the Institute of Physics for technical help. This work was supported by the Ministry of Science and Technology of China (Grants Nos. 2014CB921202, 2015CB921104, and 2016YFA0300601) and the National Natural Science Foundation of China (Grants Nos. 91321208 and 11674380). S H acknowledges support by the US NSF (Grant No. PHY-1314861) and useful discussions with Dmitri Averin.

ORCID iDs

S P Zhao https://orcid.org/0000-0003-2120-8356

References

[1] Clarke J and Wilhelm F K 2008 *Nature* **453** 1031
[2] Devoret M H and Schoelkopf R J 2013 *Science* **339** 1169
[3] Semenov V K, Danilov G V and Averin D V 2003 *IEEE Trans. Appl. Supecond.* **13** 938
[4] Semenov V K, Danilov G V and Averin D V 2007 *IEEE Trans. Appl. Supecond.* **17** 455
[5] Ren J, Semenov V K, Polyakov Y A, Averin D V and Tsai J S 2009 *IEEE Trans. Appl. Supecond.* **19** 961
[6] Ren J and Semenov V K 2011 *IEEE Trans. Appl. Supecond.* **21** 780
[7] Li H, Liu J S, Zhang Y S, Cai H, Li G, Liu Q C, Han S and Chen W 2017 *Supercond. Sci. Technol.* **30** 035012
[8] Deng Q and Averin D V 2014 *J. Exp. Theor. Phys.* **119** 1152
[9] Averin D V, Xu K, Zhong Y P, Song C, Wang H and Han S 2016 *Phys. Rev. Lett.* **116** 010501
[10] Ankerhold J and Grabert H 2003 *Phys. Rev. Lett.* **91** 016803
[11] Su F F, Liu W Y, Xu H K, Deng H, Li Z Y, Tian Y, Zhu X B, Zheng D N, Lu L and Zhao S P 2017 *Chin. Phys.* B **26** 060308
[12] Martinis J M, Nam S, Aumentado J and Urbina C 2002 *Phys. Rev. Lett.* **89** 117901
[13] Tian Y *et al* 2012 *Rev. Sci. Instrum.* **83** 033907
[14] Yu H F *et al* 2011 *Phys. Rev. Lett.* **107** 067004
[15] Tinkham M 1996 *Introduction to Superconductivity* (New York: McGraw-Hill)
[16] Dutta P, Adhikari S and Bhattacharyya S P 1993 *Chem. Phys. Lett.* **212** 677
[17] Wang H *et al* 2009 *Appl. Phys. Lett.* **95** 233508
[18] Wenner J *et al* 2011 *Appl. Phys. Lett.* **99** 113513
[19] Sage J M, Bolkhovsky V, Oliver W D, Turek B and Welander P B 2011 *J. Appl. Phys.* **109** 063915
[20] Megrant A *et al* 2012 *Appl. Phys. Lett.* **100** 113510
[21] Bruno A, de Lange G, Asaad S, van der Enden K L, Langford N K and DiCarlo L 2015 *Appl. Phys. Lett.* **106** 182601
[22] Liu Y X, You J Q, Wei L F, Sun C P and Nori F 2005 *Phys. Rev. Lett.* **95** 087001
[23] Han S, Lapointe J and Lukens J E 1989 *Phys. Rev. Lett.* **63** 1712
[24] Li S X, Yu Y, Zhang Y, Qiu W and Han S 2002 *Phys. Rev. Lett.* **89** 098301
[25] Balestro F, Claudon J, Pekola J P and Buisson O 2003 *Phys. Rev. Lett.* **91** 158301